Fiber Optic Acoustic Sensor Based on SMS Structure With Thin Polymer Diaphragm for Partial Discharge Detection

L. G. PAVAN KUMAR CHAGANTI [ID]1, MOHD HAFIZI AHMAD [ID]1, (Member, IEEE), MOHAMED AFENDI MOHAMED PIAH1, MUHAMMAD YUSOF MOHD NOOR2, AND ASRUL IZAM AZMI2

1Institute of High Voltage and High Current (IVAT), School of Electrical Engineering, Faculty of Engineering, Universiti Teknologi Malaysia, Johor Bahru 81310, Malaysia
2Department of Communication Engineering, School of Electrical Engineering, Faculty of Engineering, Universiti Teknologi Malaysia, Johor Bahru 81310, Malaysia

Corresponding author: Mohd Hafizi Ahmad (mohdhafizi@utm.my)

ABSTRACT This paper proposes a fiber optic acoustic sensor (FOAS) based on a single-mode fiber - multimode fiber - single-mode fiber (SMS) structure attached to a thin polymer film used as a diaphragm. The diaphragm was specially developed to enhance the sensitivity towards the acoustic pressure-wave resulted from the partial discharge (PD) events. The sensitivity and signal-to-noise ratio (SNR) characterizations of the FOAS without and with a thin polymer film were performed. Both time-resolved and phase-resolved partial discharge (PRPD) patterns measurements were carried out in air and oil media. The experiment was conducted with three-electrodes using FOAS in conjunction with the conventional PD measurement as per IEC 60270 standard. The sensor achieved a sensitivity up to -31.21 dBm and -30.8 (0 dBm is defined as $1V/\mu$Bar) using broadband and tunable light source, respectively. The discharge characteristics pattern of FOAS was verified with IEC 60270 standard, and the patterns of FOAS resembled IEC 60270 standard. The proposed FOAS was capable for detecting the PD using both broadband and tunable laser lights. The use of the thin polymer film had a significant impact on the acoustic sensitivity. With the simple, low-cost design structure and free from electromagnetic interference, FOAS is found to be suitable as an in-situ sensor for detecting the acoustic signals of partial discharge and can be utilized inside the transformer.

INDEX TERMS Polymer, phase-resolved partial discharge, SMS, and surface discharge.

I. INTRODUCTION

The power transformer and switchgear are the key equipment in the power systems and traction systems. In general, the life of the power transformer is around 40 years under the normal proper maintenance condition. The failure in the power transformer is usually triggered by causes such as partial discharge, deterioration of the insulation, overheating moisture, winding resonances, lighting strikes, short circuit and other incidents [1]. The life span of these equipment is determined by evaluating the status of insulation [2]. Due to ageing, the dielectric insulations presented in these equipment get deteriorated. The ageing reduces the insulation capacity to withstand these electrical, thermal and mechanical stresses,

which are inevitable and eventually leads to catastrophic failure of the equipment. The cost required to repair a power transformer is not only expensive but time consuming. The high voltage equipment needs to be monitored continuously for the identification of insulation degradation in the early stage to avoid catastrophic failure [3].

The sign of the insulation deterioration is monitored by identifying the PD activity. The PD emitted from the insulation defect reflects the condition of the transformer [4]–[8]. The PD can be monitored via offline and online monitoring systems. Nowadays, the advancement in technology and operational safety, the online monitoring is becoming necessary. The online PD measurement has been conducted via unconventional methods by using sensors such as High-Frequency Current Transformer (HFCT), Ultra-high frequency (UHF), Transient Earth Voltage (TEV), and

Piezoelectric Transducer (PZT). These are accessible to provide continuous monitoring of the systems. However, these methods are facing the problem of electromagnetic interference and fault alarms due to environmental disturbances. The environmental and physical factors, such as temperature, humidity, voltage, pressure, chemical changes, and load, influences the PD activity. By observing the changes in the above parameters by online and offline methods, the status of insulation can be evaluated. PD activity is typically influenced by the humidity due to presence in water vapour on the surface of the insulation, thus causing the surface PD. The high temperature and loading can cause the delamination of the mica tape of the stator winding insulation. The large delamination causes the PD to occur and, hence degrading the insulation. PD activities are proportional to voltage. When the voltage increases and exceeds the PD inception voltage of the void in the insulation, PD will be initiated and progressively increase with the increase in voltage and load. Such in the oil-filled transformer, the PD is typically detected through the existence of the hydrogen gas in the transformer oil by the dissolved gas analysis (DGA) technique. This method detects the changes in chemical (key gases) in the transformer oil. Once the hydrogen gas is above the acceptance limit as per IEC60599 and IEEE C57.104-2019 guidelines, the PD can be localized using the acoustic method.

As PD releases various types of energy such as heat, acoustic sound, light, electrical current, electromagnetic waves and chemical byproducts, PD can be detected and monitored through the changes in these energies. The PD detection methods used are acoustic detection method based on sound waves, thermovision method based on heat emission, spectrophotometry method based on light emission, DGA method based on chemical reaction changes, electrical method, TEV and UHF methods based on electromagnetic and radiofrequency radiation [9].

The acoustic method of PD detection by a piezoelectric transducer (PZT) on the transformer wall outside is currently used to identify the PD. The received signal from the internal source had significant attenuation after the signal reaching from oil to the transformer tank and to the sensor and multiple paths of the signal inside. In relation to that, the optical fiber sensor placed inside the transformer solves the above problem due to its advantages like itself acts as an insulation, immune to electromagnetic interference (EMI), long-term stability, extraordinary stability to mechanical fatigue and capable of working in a harsh environment [10].

Research of optical fiber sensors in high voltage application has gained interest in the advancement of optical measurement techniques. Among the early work was in 1991, Mangeret [11] studied the application of fluorescence optical fiber application in the gas-insulated system. Different optical measurement techniques were implemented for ultrasonic detection of PD in the transformer including Michelson interferometer (MI) [12], Mach-Zehnder interferometer (MZI) [13] and Fabry-Perot interferometer (FPI) [14] and phase-shifted fiber Bragg grating (FBG) [15]. For an

acoustic pressure of 10 Pa, the FPI had an SNR of approximately 60 dB is achievable [14]. The external FPI had a maximum amplitude of 55 dB at 36 kHz of underwater testing [16]. Ma et al. demonstrated that the sensitivity of phase shift FBG was 8.46 dB more than a conventional FBG with an average sensitivity of −63.20 dB for a range of 50 kHz to 400 kHz [15]. Blackburn found that the frequency response of the acoustical signal measured in the transformer by the sensor has a distinctive frequency range of 20 kHz to 300 kHz [17].

The sensitivity of diaphragm-based sensors depends upon the diaphragm radius and thickness [18]. Different diaphragm materials have been proposed for acoustic measurement study such as graphene [18], polypropylene/poly (ethylene terephthalate) [19], nitrile rubber [20], PDMS [21], Parylene-C [22], aluminium foil [23], gold [24], and silver [25]. The SMS structure sensors using multimode interference phenomena are gaining attention in many applications. One of the applications is acoustic sensing. It is a simple structure with a straightforward design process, operate in a wide temperature range, no necessity for the interrogator, and low cost to design as compared with FPI and FBG. Li et al. demonstrated that a single-mode-multimode (SMS) structure strain sensors were two times more sensitive than an FBG [26]. Due to these advantages, several researchers used SMS in low-frequency acoustic sensing for a frequency range below 2 kHz [27]–[29]. Meanwhile, Sun et al. used a thick aluminium foil of 2.5 cm diameter attached to SMS in detecting an acoustic signal as high as 20 kHz [30]. The conductive materials for the diaphragm might behave like a floating particle in the long run of operation, which is not optable to practice inside the transformers.

In this paper, we propose a new approach of using SMS based structure with a thin film to form a disk type in the high voltage application to detect PD. The thin polymer diaphragm is specifically developed to enhance the sensitivity over the PD acoustic signals, which is commonly being attenuated over the changes in capacitance inside the transformer. The maximum SNR for the graphite/epoxy diaphragm of fiber optic interferometric sensor was 21 dB [31]. A signal-to-noise ratio (SNR) of 43 dB was obtained by PP/PET Diaphragm at 600 Hz [19]. With a gold diaphragm for a frequency range of 20 kHz to 150 kHz, the maximum SNR achieved is 48 dB [24]. Our FOAS achieved SNR around 60 dB at 40 kHz. The research study is carried out using FOAS without and with a thin-film diaphragm to detect the acoustic signal both in air and oil media and lengthy its practice to the power transformer.

II. SENSOR FABRICATION
A. THEORY
As shown in Fig. 1, the SMS consists of a short multimode fiber (MMF) in between two single-mode fiber (SMF) fiber sections. When light entering the MMF from SMF, it is excited into higher-order modes that propagated along the
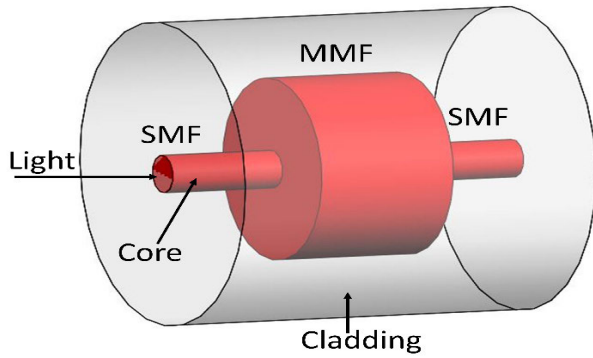
FIGURE 1. SMS interference structure.

FIGURE 2. The change in the center deformation of the polyester film with pressure change.

MMF at different velocities. The acoustic pressure acting on the polymer diaphragm generates vibration of the diaphragm. The vibration results in a change of length of MMF in SMS. The mode propagation in the MMF is sensitive towards bending of MMF. At the end of MMF, the power coupled to the SMF output highly sensitive to the intensity shift between multiple modes. The interference caused by the acoustic vibration acting on the MMF results in the phase alteration of the light propagating in the fiber, which in turn measured as the intensity at output SMF.

The fundamental mode field distribution for the input light, $E(r,0)$ in the SMF with circular symmetrical features [32]. Assumed a perfect axes alignment between the lead in SMF and MMF cores, the fundamental mode in SMF is further decomposed into LP_{0m} modes excite and travel in the MMF from lead in SMF. Now, assuming the field profile of LP_{0m} as $P_m(r)$ and the input field distribution in MMF is given as;

$$E(r, 0) = \sum_{m=1}^{M} C_m P_m(r) \qquad (1)$$

where C_m is the coefficient of the exciting modes, M is the total number of modes, and $P_m(r)$ is eigenmodes in the MMF. Hence, the coefficient of the fundamental mode between the mth order mode of MMF and SMF can be stated as;

$$C_m = \frac{\int_0^\infty E(r, 0) P_m(r) r dr}{\int_0^\infty P_m(r) P_m(r) r dr} \qquad (2)$$

The output power from the SMS structure, $L_s(z)$ is obtainable as follows [33], [34]:

$$L_s(z) = 10 \log_{10}\left(\left|\sum_{m=0}^{M} C_m^2 e^{(i \beta_m (z - \Delta z))}\right|^2\right) \qquad (3)$$

where the z is the length of MMF, and β_m is the propagation constant of the mth order mode.

The polyester film diaphragm design plays a vital role in the sensitivity of the sensor. The load-deflection relation is the primary method for the determination of elastic properties of polyester film. The center deformation of the polyester film
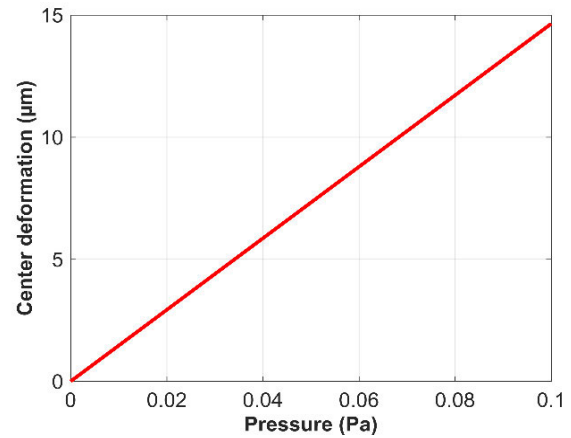
diaphragm that is rigidly clamped is given as [19]:

$$\Delta z = \frac{3p(1 - \mu^2) r_p^4}{16Y t_d^3} \qquad (4)$$

where μ, Y, t_d and r_p are the Poisson's ratio, Young's modulus, thickness and radius of the polymer film, respectively. p and f are the applied sound pressure and frequency of an acoustic wave, respectively. This deformation leads to a quick release of energy in the form of elastic waves or acoustic emissions. These rapid energy-releasing waves with frequencies in the range of ultrasonic. This AE is generated from material degradation, reversible processes, fabrication process, leak, and flow processes [35]. In theoretical analysis, the following values are assumed: $\mu = 0.49$, $Y = 4100$ MPa, $r_p = 1.5$ cm and $t_d = 23$ μm. The pressure is varied from 0 Pa to 0.1 Pa. The change of the center deformation of the polyester film with the applied pressure is linear, as shown in Fig. 2. The center deformation observed is 0 to 15 μm for 0 to 0.1 Pa pressure change.

B. FOAS WITHOUT POLYMER FILM FABRICATION
The MMF and SMF sections were spliced using an automatic function in fusion splicer (Furukawa S178A). The SMF and MMF (core, cladding) size used were (9 μm, 125 μm) and (105 μm, 125 μm), respectively. The length of the MMF section was 5 cm.

C. FOAS WITH A POLYMER FILM FABRICATION
A polyester film of 23.5 μm thickness was used in the design, as shown in Fig. 3b. This polymer film was selected due to its advantages that suitable for the PD measurement requirement. It remains flexible and tough for a wide temperature range between -70 °C to 150 °C. It has high tensile strength, dielectric strength, tear, and impact stress. It shows excellent resistance to moisture and most chemicals in industries. The polyester is used as an electrical and thermal barrier in transformers, motors, and cables. Firstly, an SMF was sewn in the polymer film with a gap between each sewing was done
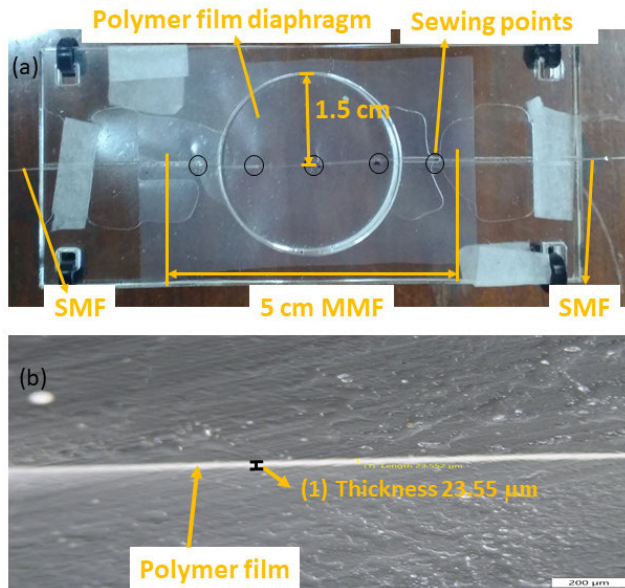
FIGURE 3. (a) Fabricated FOAS with a thin polymer film (b) microscopic image of polymer.

with 1 cm gap, then this SMF and MMF are spliced in a similar procedure of SMS followed. The other end of MMF was spliced with SMF. Next, the polymer film was slowly moved from SMF fiber to MMF fiber. The Polyester film of 4 cm × 6 cm rectangular shape was used, which forms a 1.5 cm radius diaphragm. Lastly, two acrylic rectangular plates of length 9 cm and breadth 5 cm with a hole of 1.5 cm radius at the center were sandwiched on the SMS, as shown in Fig. 3a, which is FOAS with a polymer film diaphragm. From equation 4, the change in the center deformation ∇d is proportional to the radius of the diaphragm and inversely proportional to the thickness. The sensitivity of the sensor increases by increasing radius and reducing the thickness of the diaphragm [19], [22]. The thickness cannot be too thin, and it can be easily damaged. At the same time, the radius should not exceed much to limit the size of the sensor to place inside a narrow space such as inside a transformer.

III. FOAS CHARACTERIZATION USING ACOUSTIC TRANSMITTERS
A. METHODOLOGY USING AIR CERAMIC TRANSDUCER
The air ultrasonic ceramic transmitters with center frequency at 40 kHz and 75 kHz were used to identify the frequency response and SNR of the FOAS. The experimental setup is shown in Fig. 4. A gap of 2 cm was maintained between the transmitter and the sensor initially, and it was increased up to 16 cm. A GW audio generator (model GAG-808G) was used to supply a tonal signal to the transmitter. The sensor output from the photodetector (PDA10CS-EC InGaAs Amplified Detector 700-1800 nm) was sent to the data acquisition (DAQ) unit. The DAQ consists of NI SCB-68 I/O connector block, which is connected to a PC with a NI DAQ card and LABVIEW software. Sensor feasibility was evaluated by using two types of light sources; a broadband source (BBS,
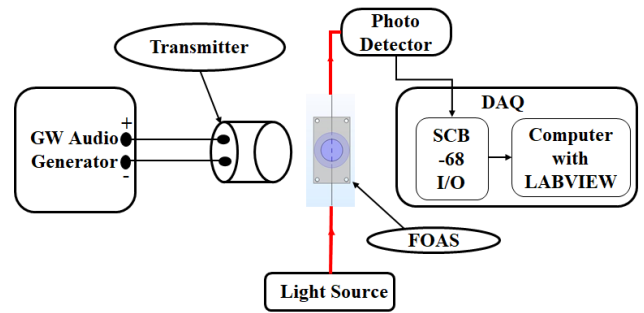

FIGURE 4. Schematic view of the experimental set up using a transmitter.

Model ASE-C-GFF-10) and a tunable light source (TLS, Model Agilent 81689A). The GW audio generator provides the input to the air ceramic transducer with center frequency at 40 kHz.

Initially, BBS and optical spectrum analyzer (OSA) are used to test the FOAS output spectra. Secondly, the acoustic pressure generated by the transmitter at a frequency of 40 kHz ± 1 kHz is placed 2.5 cm away from the FOAS. The BBS light was launched into the FOAS, the data was recorded with the DAQ first by varying frequency, and then after by varying the distance between the FOAS and transmitter from 2 cm to 16 cm by fixing constant frequency. Thirdly, the TLS was launched into the FOAS and selected the wavelength at which the FOAS had the highest sensitive response and continued the second step. Finally, repeat the last two stages of the experiment procedure with the 75 kHz acoustic transmitter. While data acquisition, no gain is applied at photodetector for BBS and a 20 dB gain used for TLS. The 40 kHz and 75 kHz are used in the experiment due to the following facts; In air medium, there is significant evidence that at 40 kHz frequency, the PD signals occur and free from the ambient noises [36], [37]. There are several recommendations from the leading manufactures for the optimal detection of the PD in the oil-filled transformer. Some recommended PZT are VS30 (20–80 kHz), VS75 (30–120 kHz, frequency resonant at 75 kHz), and type R15i (50 kHz to 400 kHz, resonant frequencies: 75 kHz and 150 kHz) [38].

B. RESULTS AND DISCUSSION
The transmission spectra of the FOAS are shown in Fig. 5. The signal power of the sensor with polymer is lower when compared to the sensor without polymer due to bending loss caused by zigzag sewing of fiber through the film. As the length of MMF increases, this increases the number of spatial modes beating in the MMF; thus, the transmission spectrum comb pattern will become more prominent. However, Masnan *et al.* observed, the length does not significantly influence the sensitivity of the sensor [39]. When the length of the MMF exceeds the acrylic rectangular plates length, the transmission loss of the MMF fiber is adversely affected by outside interferences or free end of MMF unstable in free space or inside transformer due to oil flow. In the experiment, the length of MMF was fixed at 5 cm, then the SMF and MMF
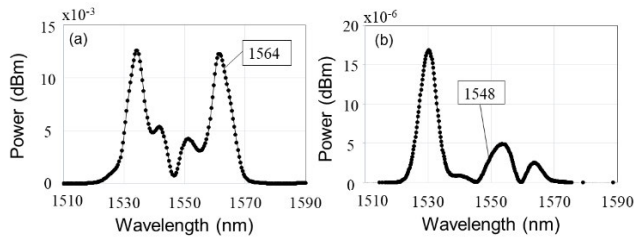
FIGURE 5. Transmitted spectrum for the FOAS (a) without and (b) with a thin polymer film under no acoustic pressure condition.
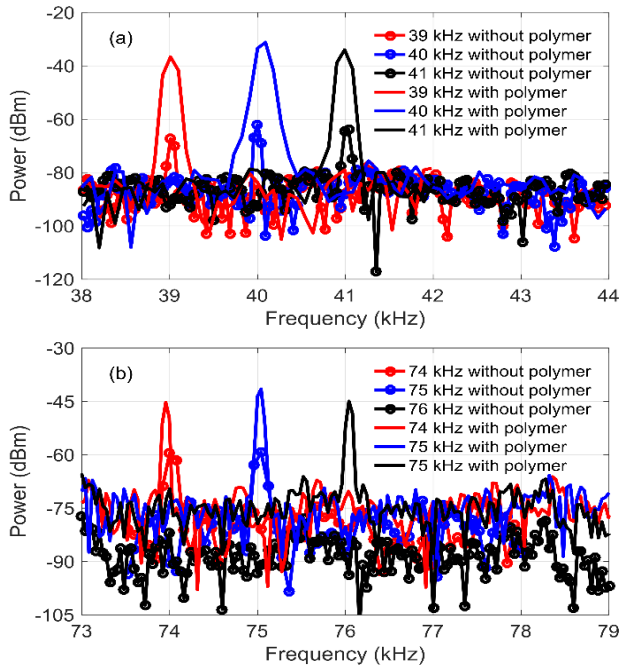

FIGURE 6. FFT response of FOAS using the transmitter with center frequency at (a) 40 kHz and (b) 75 kHz with BBS light and a gap of 2.5 cm maintained between FOAS and transmitter.

FIGURE 7. FFT Response of FOAS using BBS by distance variation between source and FOAS with transmitter center frequency at (a) 40 kHz and (b) 75 kHz.

FIGURE 8. FFT response of FOAS using TLS with 2.5 cm apart between source and sensor FOAS.

splicing joint were inside the acrylic plates, it can protect from mechanical damages or avoid bending of the SMF and MMF joint. Moreover, the size of the sensor should not be large to put in the transformer. Fig. 6 shows the FFT response of FOAS with and without the polymers around the resonance frequency of the transmitter, i.e., 40 kHz and 75 kHz and a driving voltage of 0.1 V applied to the transmitter. The attained sensitivities at 40 kHz for FOAS with polymer was −31.21 dBm, and without polymer was −62.09 dBm (0 dBm is defined as 1V/μBar). While at 75 kHz, the sensitivities were −47.52 dBm and −59.26 dBm for FOAS with and without polymer, respectively, using BBS.

It is evident that FOAS with a polymer thin film produced higher sensitivity compared to FOAS without polymer. In addition, the sensitivity at 40 kHz and 75 kHz are higher than the other frequencies because the transmitter's resonance are at 40 kHz and 75 kHz. The sensor response against varying distance from the source is shown in Fig. 7. The maximum distance that FOAS without polymer can detect
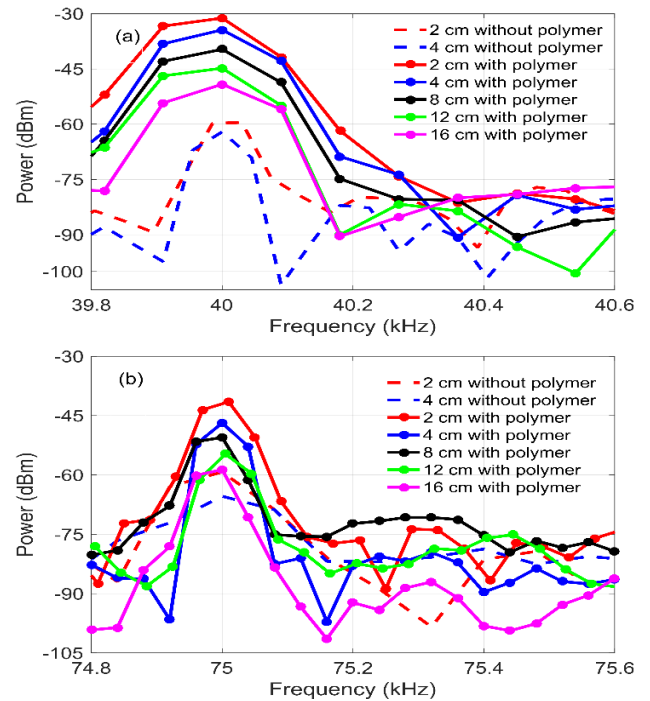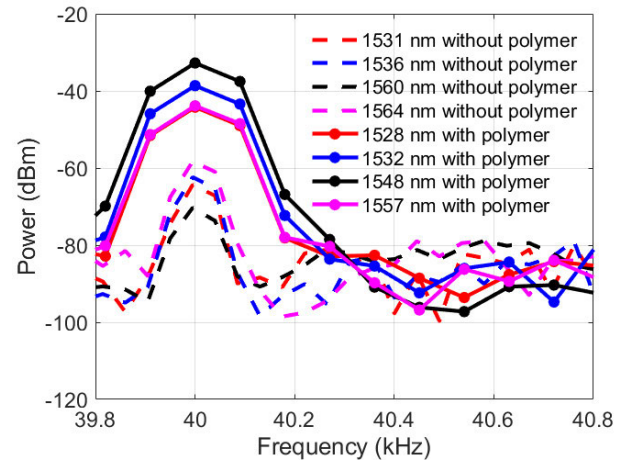
signal is 4 cm, and beyond that, it fails to sense the acoustic waves. Meanwhile, FOAS with polymer detects the emission as far as 16 cm from the source with SNR near to 30 dB, and it can sense signal with further increase in the distance. The signal power level at the dynamic range reduces almost in a linear manner as the distance between the sensor and source increases.

TLS wavelength was set at the most sensitive point of the sensor spectra, i.e., 1564 nm for FOAS without polymer and 1548 nm for FOAS with a polymer film based on Fig. 8 results.

The FOAS with polymer film has shown significant sensitivity enhancement compared to FOAS without polymer film.
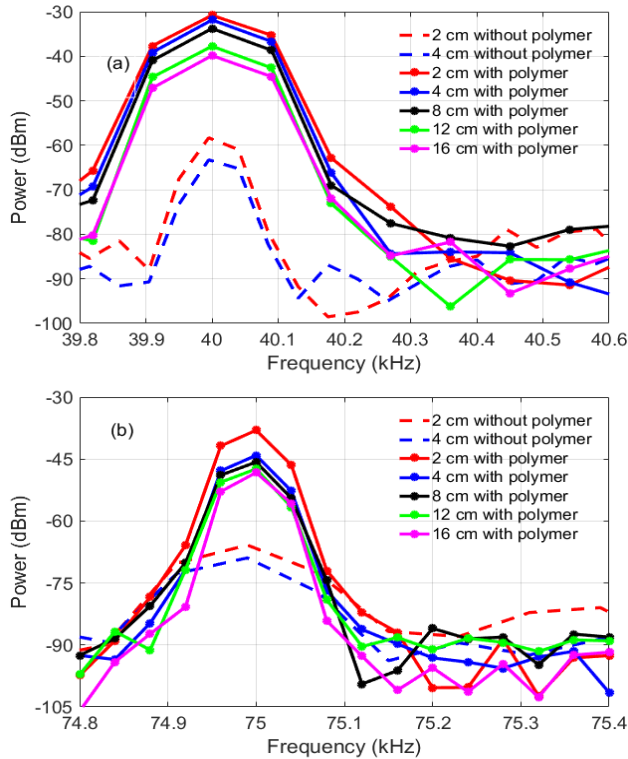
FIGURE 9. FFT Response of FOAS using TLS with a wavelength of 1564 nm without a polymer and 1548 nm with polymer film at center frequency (a) 40 kHz and (b) 75 kHz.

FIGURE 10. The signal to noise ratio with varying distance between the source and FOAS (a) without polymer film and (b) with a thin polymer film.

As the distance increases, the power of the signal decreases. This is due to the spreading of the acoustic wave over a larger area and absorption loss of acoustic signal. As shown in Fig. 9, the signal detection using FOAS without a polymer film is limited up to 4 cm range only, whereas FOAS with a polymer film can go more than 4 times the distance. It absorbs the maximum amount of energy from the acoustic pressure and provides a higher center deformation of MMF fiber as compared with FOAS without polymer film. Using TLS, the sensitivity achieved by FOAS with and without polymer film at 40 kHz was −30.8 dBm and −58.31 dBm (0 dBm is defined as $1V/\mu Bar$). Similarly, the sensitivities at 75 kHz are −38.02 dBm and −66 dBm.

Fig. 10 shows the SNR against distance for different investigated schemes. The SNR of the FOAS with polymer film at 40 kHz and 75 kHz is in between 2 to 2.5 times more than FOAS without polymer film at 4 cm. The FOAS structure using polymer film has better performance due to the large radius of the polymer film, thermal stability up to 150 °C makes it suitable for the harsh environment in the transformer. The FP interferometer is limited to use only TLS for PD detection [40]–[42]. This FOAS sensor is competent to utilize both TLS and BBS as its light sources.

IV. APPLICATION IN PD MEASUREMENT
A. PD EXPERIMENTAL SETUP
A high voltage supply was applied to the test cell for the PD generation. It was carried out by placing barrier insulation
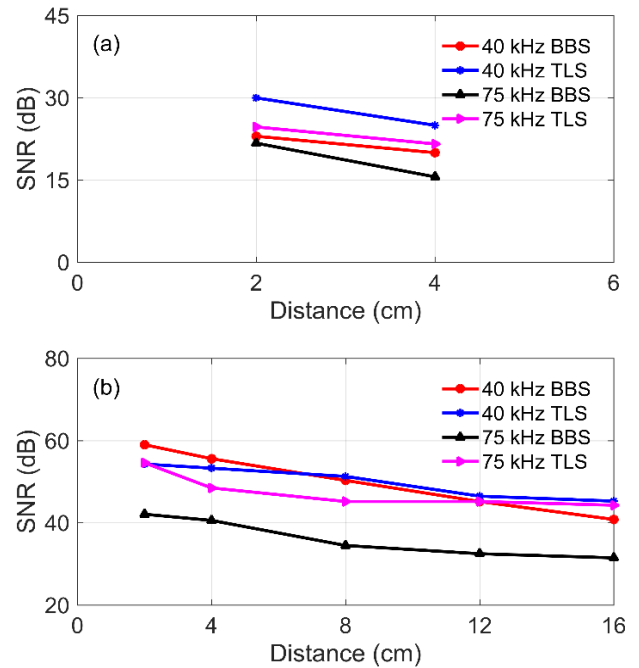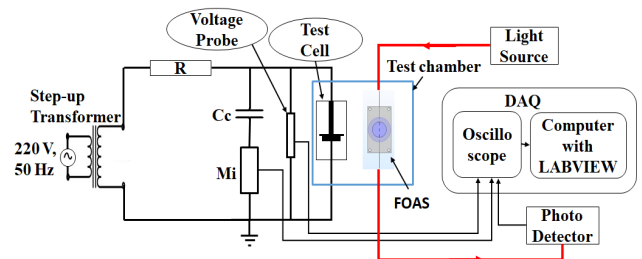

FIGURE 11. Experimental setup for PD measurement.

of low-density polyethylene (LDPE) with 1 mm thickness between the electrode and ground plate. The three different types of electrodes were utilized to generate surface discharge. A 220 V, 50 Hz was supplied to the BAUR voltage regulator, and it was stepped up to between 0-100 kV using a transformer. A 60 W, 6100 Ω current limiting resistor was connected in series with the transformer and the test cell in order to limit the breakdown current in case of a breakdown occurs. The AC supply voltage was measured using a voltage probe (Tektronix P6105A) that was connected to an oscilloscope (Tektronix TDS3034B). The experimental setup for PD measurement is shown in Fig. 11. Measurement data was collected from the oscilloscope using LABVIEW software.

The PD magnitude was measured using a measuring impedance with a coupling capacitor adopting the IEC60270 standard and in parallel with FOAS. The light source is applied to the input of FOAS, and output was collected by photodetector and DAQ. The coupling device consists of a coupling capacitor (C_C = 1 nF), and a measuring impedance (M_i) were connected in series and parallel to the
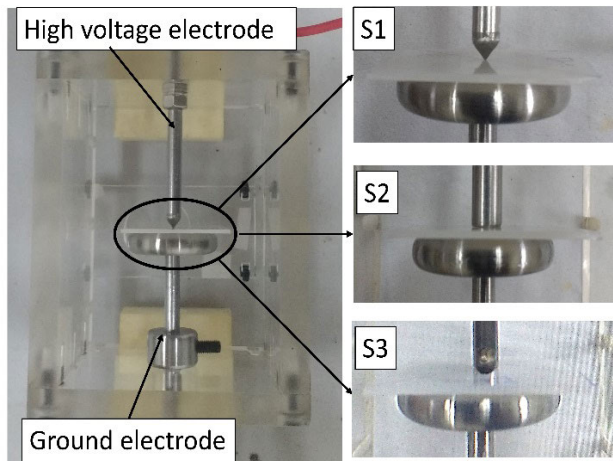
FIGURE 12. Test cell used for PD measurement with different electrodes configuration S1, S2 and S3.

FIGURE 13. PRPD from FOAS using (a) BBS and (b) TLS type light source in the (i) air and (ii) oil media.

test object. By using a PD calibrator, the circuit was calibrated by injecting a known amount of the charge into the circuit between 200 and 2000 pC. For IEC60270, the frequency range chosen for measuring PD is 30kHz to 1 MHz. The phase and charge magnitude of PD pattern analysis are recorded to assess the discharge patterns.

The process of executing the experiment is as follows: Before performing the experiment, the test setup was calibrated by injecting a known charge value (pC) across the terminal of the test cell using Haefely PD calibrator type 451, and DAQ recorded the apparent charge. The ground electrode was a plain plate of 3 cm in diameter. The HV electrode used with three configurations referred to as a needle-plane (S1), IEC (b) electrode-plane (S2) and spherical-plane (S3) as shown in Fig. 12.

In the air medium, a voltage of 7.5 kV AC was applied across the test cell, and the PRPD patterns were recorded for 60 minutes using FOAS and coupling device. The process was reiterated using the other electrode shapes. In the oil medium, both the test cell and FOAS were placed in a tub containing silicone oil and a voltage of 11.5 kV AC was applied across the test cell. The experiment execution procedure was the same as in the air medium.

B. TEST FOR PD MEASUREMENT

The PD signals result in impulse force on the insulation, thereby causing high-frequency oscillation and consequent acoustic wave production, which are longitudinal compressive waves. The acoustic signal level depends on the acoustic path, which is influenced by the absorption such as dissipation, scattering of the acoustic energy in medium and spatial attenuation. This attenuation is dependent on the geometrical effect of the source and the shape of the transmitting medium such as air, SF6, polymer or oil. Also, reflections and refractions at the boundaries can cause attenuation, absorption, and scattering effects as well. As the signals travel, the attenuation factor can be in a factor of $1/\sqrt{x}$ which x is the distance
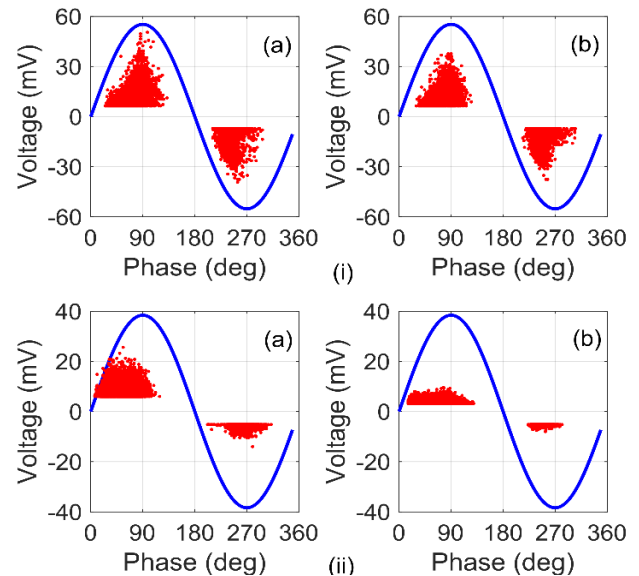
from the PD source. The PRPD pattern analyses the PD signal distribution.

The maximum dielectric stress tolerates by the insulation material is termed as dielectric strength. The dielectric strength of the insulation material was affected by the various parameters such as temperature, the shape of the electrodes, type of the voltage applied, moisture quantity, and impurities. The significant faults happen due to the voids inside the insulation and surface discharge on the insulation material. This surface discharge may create continuous conducting paths called tracking. In practice, it is not wholly possible to eliminate the PD, but precaution measurements are possible to increase the life expectancy of the equipment [43]. In view of the foregoing, the S1, S2 and S3 electrodes were used with a barrier in between the electrodes to generate surface discharges. The effect of the high electrical stress at the protrusion tip of the conductor produces the electrons and discharge at the interface of conductor and insulation medium. The starting electron can be created from the photoionization, UV or cosmic irradiation or from electron detachment from the metal surface. All these mechanisms eventually lead to Townsend and streamer discharges; thus, consequently, create conduction current, which is cumulatively measured through the coupling device. The PRPD, time-domain data in the air and oil media are studied and discussed.

To choose which type of light source is preferable for the PRPD measurement, the experiment performed for 60 minutes using both BBS and TLS are shown in Fig. 13 under the similar condition of voltage. The results show that FOAS using the BBS had higher sensitivity than TLS type at 1548 nm wavelength, both in the air and oil media. From these results, the rest of the experiments are carried out with a BBS type light source. For the tunable laser, the focus is on only one particular wavelength of power
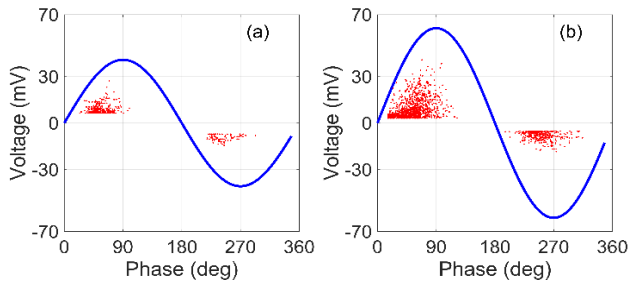
FIGURE 14. PRPD of FOAS (a) without polymer film and (b) with a thin polymer film.
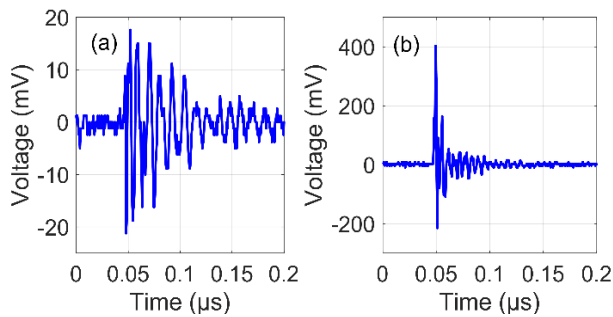

FIGURE 15. Typical time-domain PD pulse signal in air media using S1 electrode configuration (a) FOAS and (b) IEC 60270.

FIGURE 16. PRPD patterns obtained due to surface discharge in the air medium (a) FOAS and (b) IEC 60270 using (i) S1 (ii) S2 and (iii) S3 electrode configurations.

changes. The acoustic vibrations are fast, and the difference in the power observed at that point of wavelength changes faster. It is challenging for the DAQ to identify the rapid changes at that specific point. Due to this might be, BBS is more sensitive than TLS. Fig. 14 shows the result of FOAS without the polymer and with polymer under similar conditions. The signal captured from FOAS without polymer film was less sensitive in terms of the amplitude, the number of PD pulses detecting, and phase are also narrow.

In the air medium, the typical time-domain PD signal with S1 configuration is shown in Fig. 15. The output signal of the OFS is 38.8 mV$_{p-p}$ and for IEC60270 is 618 mV$_{p-p}$ where V$_{p-p}$ is peak to peak voltage. The PRPD patterns recorded from the FOAS with a polymer film and simultaneously with the IEC60270 standard are presented in Fig.16.

For the PD pulses in the time domain, the acoustic signal exits for a longer time than the signal captured from the IEC60270. This is because the sound wave travels in the air with a speed of around 343 m/s at 20 °C while the charge-discharge in nanoseconds duration. The FOAS output was recorded in the form of a voltage (V)-phase, and IEC60270 data were recorded in charge (Q)-phase. Since the IEC60270 measurement is related to integral of PD current pulse, whereas the data from FOAS are dependent on the acoustic signal. Due to differences in properties and detection mechanisms, no relation between acoustic and electrical signal, thus no calibration procedure has been adapted for unconventional PD method. Only, sensitivity or performance check has been explained in the IEC TS 62478 standard. The voltage signal obtained from the FOAS to charge (Q)
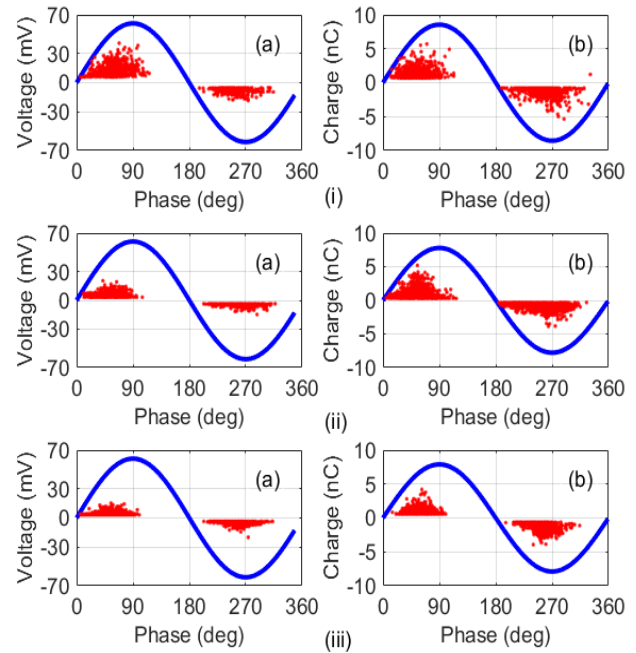
conversion is not possible. According to the PRPD diagrams, the discharge characteristics from both measurement methods resemble asymmetrical patterns.
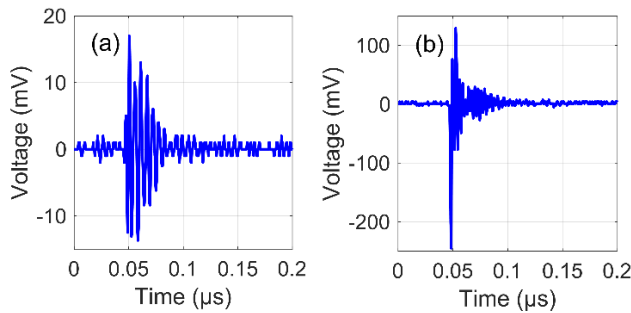
The phase of the signal recorded lies in the range of 10 to 110 degrees in the positive cycle, 180 to 330 degrees in the negative cycle of the applied voltage in the FOAS and IEC60270 measurement. The maximum discharge magnitudes of the signal in the positive cycle for the FOAS were 40.8 mV, 20.4 mV and 15.2 mV for S1, S2 and S3 electrodes, respectively. In the negative cycle, the values were −18.4 mV, −14.8 mV and −14.4 mV, respectively, for S1 to S3 patterns in air medium. The change in the signal amplitude for S1 to S3 in the positive half cycle is recognizable, whereas in the negative cycle minute. In IEC 60270, the maximum PD discharge values for S1 to S3 electrodes in the positive cycle were 5.70 nC, 5.19 nC, and 4.21 nC and in negative cycle −5.35 nC, −3.86 nC and −3.64 nC respectively. The noise level for the FOAS is 5 mV for all the electrode in air and oil medium. In the IEC method, the noise level for S1, S2 and S3 electrodes in air medium is in between 100-110 pC. The discharge patterns in both cycles are asymmetrical in all measurements from the values, as shown in Table 1, indicating surface-type discharge.

In the oil medium, data was recorded in a similar way as in an air medium. The typical time-domain signal was shown in Fig. 17 for the S1 electrode. The output signal amplitude of the FOAS is 30.7 mV$_{p-p}$ and for IEC60270 is 374 mV$_{p-p}$. The FOAS signal amplitude is lower than the pulse detected using IEC 60270 method. This is due to the applied broadband light source power is mW, and for IEC 60270, the signal was directly measured from the coupling device. The phase of the

TABLE 1. PD in positive and negative cycles in air medium

	FOAS				IEC 60270			
E_s	P_{PDs}	N_{PDs}	R_{max}	A_{PD}	P_{PDs}	N_{PDs}	R_{max}	A_{PD}
S1	654	336	2.21	2.4	954	840	1.06	2.3
S2	1304	432	1.37	2	1322	1250	1.34	3.2
S3	2016	859	1.05	3.5	2165	910	1.14	3.4

E_s= Electrode shape, P_{PDs} = number of PD in positive cycle, N_{PDs} = number of PD in negative cycle R_{max}= The ratio of maximum PD amplitude in positive and negative cycles, A_{PD}= Average number of PD per cycle.

TABLE 2. PD in positive and negative cycles in oil medium

	FOAS				IEC 60270			
E_s	P_{PDs}	N_{PDs}	R_{max}	A_{PD}	P_{PDs}	N_{PDs}	R_{max}	A_{PD}
S1	3202	2614	0.90	5.0	2290	2711	1.09	11.9
S2	1575	583	1.13	14.0	2540	2461	0.87	19.0
S3	4679	1093	1.47	5.0	3523	1478	1.35	12.5

FIGURE 17. Typical time-domain PD pulse signal in oil media using S1 electrode configuration (a) FOAS and (b) IEC 60270.
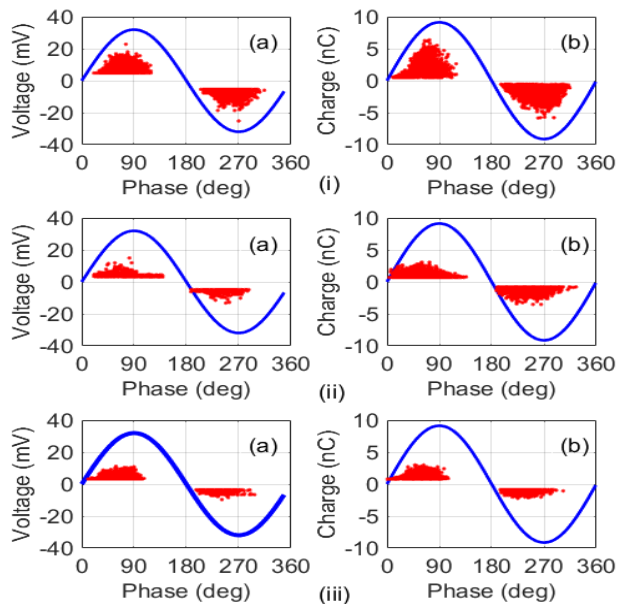
FIGURE 18. PRPD patterns obtained due to surface discharge in the oil medium (a) FOAS and (b) IEC 60270 using (i) S1 (ii) S2 and (iii) S3 electrode configurations.

signal lies in the range of 0 to 138 degrees in the positive cycle, 183 to 325 degrees in the negative cycle of the applied voltage for both the IEC60270 method and the FOAS. The amplitudes of the PD discharge decreased from S1 to S3 for both the detection methods, as shown in Fig. 18.

In FOAS, the maximum values for S1 to S3 in the positive cycle were 22.8 mV, 14.96 mV, 11.2 mV and in the negative cycle were −25.2 mV, −13.2 mV, −9 mV, respectively. In IEC 60270, the maximum PD magnitude values for S1 to S3 in the positive cycle were positive PDs with magnitudes of 6.38 nC, 3.07 nC, 2.99 nC and in negative cycle of negative PDs were −5.83 nC, −3.5 nC, −2.21 nC, respectively. The noise level in the oil medium for the IEC method is around 100-120 pC. From Table 2, the PRPD patterns are asymmetrical.

Moreover, the field enhancement factor (f_f) is the ratio of the maximum electric field (E_m) to average electric field value (E_{av}). The field enhancement factor (f_f) for the electrodes S1, S2 and S3 are 9.55, 1.82 and 0.79, respectively. Therefore, the E_m at the tip of the electrode for S1 to S3 are $9.55E_{av}$ kV/mm, $1.82E_{av}$ kV/mm and $0.79E_{av}$ kV/mm. The E_{av} is the applied ac rms voltage, 7.5 kV in air and 11.5 kV in oil media, respectively.

For the S1 to S3 electrode setups, the PD discharge amplitude of the signal descends from S1 to S3 in air and oil media. The main reason for this is the shape of the electrode and explained as follows. The S1 creates a high intensified non-uniform electric field by the sharp tip of the needle, due to the high f_f and E_m, which creates an intense impact on the surface of the insulation causing higher PD. This might lead to streamer's formation over the surface of the insulation. The S3 produces a quasi-uniform electric field because of the smooth curvature, and S2 produces a more non-uniform electric field than S3 due to the corner edge shape of the electrode. The E_m depends on the type and the radius of the protrusion, as the radius of the protrusion decreases, the field will be maximum. The amplitude of the signal is slightly low in the oil medium for FOAS due to the reradiation of acoustic energy. This happened when a diaphragm was immersed in a liquid medium due to the extra added mass effect when compared with the air medium [16].

The asymmetry in FOAS was dominant than IEC method, this might be due to loss of acoustic signal energy in medium while travelling from the source to FOAS. The impedance offered by the liquid medium to the acoustic signals is higher than the air medium. Not only this, but the dielectric strength of the oil was also higher than the air, and it requires higher PD inception voltage to generate PD. The FOAS PRPD pattern using S1 had the same pattern as the IEC60270 method, and for the latter cases S2 and S3, its amplitude reduces in both media. For all measurements, the PRPD patterns are asymmetrical in both the positive and negative cycles with variation in the PD pulse count, as shown in Tables 1 and 2.
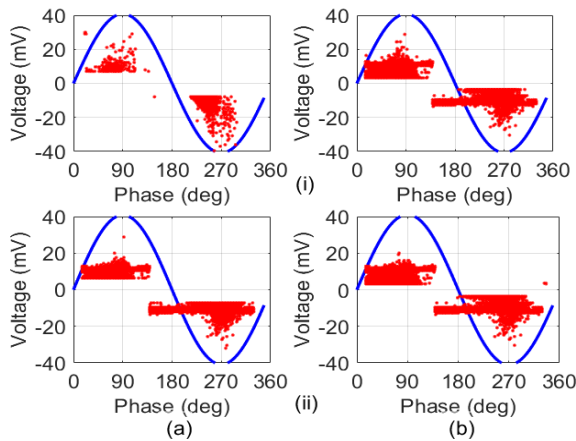
FIGURE 19. PRPD patterns in (a) air and (b) oil obtained by varying the spacing between source and FOAS (i) 4 cm and (ii) 8 cm.

Fig. 19 shows the PRPD data with the variation of the distance between the sensor and the PD source. There is a slight reduction (attenuation) in the amplitude of the signal in both positive and negative cycles with the increase of spacing between the source and FOAS.

These results are supported by the following previous research works as follows. Rahman *et al.* studied the effect of Cu particles in oil by varying the electrode configuration and particle size [44]. Rahman concluded that the magnitude of the pulses depends on the shape of the electrode. Also, Firuzi *et al.* investigated the corona, surface discharge in air and oil medium using radiofrequency and IEC60270 techniques, and concluded PD recorded by the surface discharge in the air had a higher amplitude than in oil [45]. As for the application, FOAS can be placed close to the transformer winding to detect the PD coming from that region, as a similar position as RTD or fiber optic based temperature sensor, which placed to detect winding temperature for the triggering an alarm or tripping the protection relay.

V. CONCLUSION

The investigation concludes a significant impact of the thin polymer film in SMS structure for the acoustic pressure of PD detection. It shows good sensitivity of results with potential in boarding its application in all acoustic sensing. The SNR for FOAS with polymer film is 2 to 2.5 times higher than the FOAS without polymer film for both resonant frequencies of 40 kHz and 75 kHz. The FOAS was capable of detecting the signals in both air and oil media. Both light sources BBS and TLS can be used to detect acoustic pressure-waves at both frequencies and for PD detection. The FOAS without the polymer thin film diaphragm is limited up to 4 cm, and the FOAS with the polymer thin film diaphragm can detect the signal up to 16 cm and could be longer. It was observed that the broadband source usage had better sensitivity than the tunable laser source. The use of the thin polymer film in the PD detection shown a significant advantage over FOAS without polymer film diaphragm. The PRPD of the FOAS with a polymer film diaphragm comparison with the

IEC60270 standard, both follows a similar pattern for all three-electrode configurations. All electrode shapes produced surface discharges and observed asymmetrical PRPD patterns in both semi-period cycles. The acoustic signal detected in oil has a lesser amplitude than the one in the air medium. Our sensor can be further improved by investigating optimized thickness and diameter of the thin polymer film of the sensor.

REFERENCES

[1] M. Wang, A. J. Vandermaar, and K. D. Srivastava, "Review of condition assessment of power transformers in service," *IEEE Elect. Insul. Mag.*, vol. 18, no. 6, pp. 12–25, Nov. 2002.

[2] W. M. F. Al-Masri, M. F. Abdel-Hafez, and A. H. El-Hag, "Toward high-accuracy estimation of partial discharge location," *IEEE Trans. Instrum. Meas.*, vol. 65, no. 9, pp. 2145–2153, Sep. 2016.

[3] G. Paolitti and A. Golubev, "Partial discharge theory and technologies related to traditional testing methods of large rotating apparatus," in *Proc. IEEE Ind. Appl. Conf., 34th IAS Annu. Meeting*, Phoenix, AZ, USA, Oct. 1999, pp. 967–981.

[4] G. C. Montanari, "Partial discharge detection in medium voltage and high voltage cables: Maximum distance for detection, length of cable, and some answers," *IEEE Elect. Insul. Mag.*, vol. 32, no. 5, pp. 41–46, Sep. 2016.

[5] G. C. Montanari, "Time behavior of partial discharges and life of type II turn insulation specimens under repetitive impulse and sinusoidal waveforms," *IEEE Elect. Insul. Mag.*, vol. 33, no. 6, pp. 17–26, Nov. 2017.

[6] Y. Xu, X. Gu, B. Liu, B. Hui, Z. Ren, and S. Meng, "Special requirements of high frequency current transformers in the on-line detection of partial discharges in power cables," *IEEE Elect. Insul. Mag.*, vol. 32, no. 6, pp. 8–19, Nov. 2016.

[7] J. Fuhr and T. Aschwanden, "Identification and localization of PD-sources in power-transformers and power-generators," *IEEE Trans. Dielectr. Electr. Insul.*, vol. 24, no. 1, pp. 17–30, Feb. 2017.

[8] S. Ganeshan, J. Murugesan, A. Cavallini, F. Negri, B. Valecillos, and U. Piovan, "Identification of partial discharges in power transformers: An approach driven by practical experience," *IEEE Elect. Insul. Mag.*, vol. 33, no. 5, pp. 23–31, Sep. 2017.

[9] M. Kunicki, A. Cichoń, and Ł. Nagi, "Statistics based method for partial discharge identification in oil paper insulation systems," *Electr. Power Syst. Res.*, vol. 163, pp. 559–571, Oct. 2018.

[10] P. Zubiate, J. M. Corres, C. R. Zamarreno, I. R. Matias, and F. J. Arregui, "Fabrication of optical fiber sensors for measuring ageing transformer oil in wavelength," *IEEE Sensors J.*, vol. 16, no. 12, pp. 4798–4802, Jun. 2016.

[11] R. Mangeret, J. Farenc, B. Ai, P. Destruel, D. Puretolas, and J. Casanovas, "Optical detection of partial discharges using fluorescent fiber," *IEEE Trans. Electr. Insul.*, vol. 26, no. 4, pp. 783–789, Aug. 1991.

[12] J. E. Posada-Roman, J. A. Garcia-Souto, and J. Rubio-Serrano, "Intrinsic fiber optic ultrasound sensor for oil immersed detection of partial discharges," in *Proc. IEEE SENSORS*, Limerick, Ireland, Oct. 2011, pp. 386–389.

[13] Z. Q. Zhao, J. M. K. MacAlpine, and M. S. Demokan, "Directional sensitivity of a fibre-optic sensor to acoustic signals in transformer oil," in *Proc. Int. Conf. Adv. Power Syst. Control, Oper. Manage. (APSCOM)*, Hong Kong, 1997, pp. 521–525.

[14] B. Yu, D. W. Kim, J. Deng, H. Xiao, and A. Wang, "Fiber Fabry–Pérot sensors for detection of partial discharges in power transformers," *Appl. Opt.*, vol. 42, no. 16, pp. 3241–3250, Jun. 2003.

[15] G.-M. Ma, H.-Y. Zhou, C. Shi, Y.-B. Li, Q. Zhang, C.-R. Li, and Q. Zheng, "Distributed partial discharge detection in a power transformer based on phase-shifted FBG," *IEEE Sensors J.*, vol. 18, no. 7, pp. 2788–2795, Apr. 2018.

[16] S. E. U. Lima, O. Frazao, R. G. Farias, F. M. Araujo, L. A. Ferreira, J. L. Santos, and V. Miranda, "Fiber Fabry–Pérot sensors for acoustic detection of partial discharges in transformers," in *Proc. SBMO/IEEE MTT-S Int. Microw. Optoelectron. Conf. (IMOC)*, Belem, Brazil, Nov. 2009, pp. 307–311.

[17] T. R. Blackburn, B. T. Phung, and R. E. James, "Optical fibre sensor for partial discharge detection and location in high-voltage power transformer," in *Proc. 6th Int. Conf. Dielectric Mater., Meas. Appl.*, Manchester, U.K., 1992, pp. 33–36.

[18] J. Ma, H. Xuan, H. L. Ho, W. Jin, Y. Yang, and S. Fan, "Fiber-optic Fabry–Pérot acoustic sensor with multilayer graphene diaphragm," *IEEE Photon. Technol. Lett.*, vol. 25, no. 10, pp. 932–935, May 15, 2013.

[19] L. Liu, P. Lu, H. Liao, S. Wang, W. Yang, D. Liu, and J. Zhang, "Fiber-optic michelson interferometric acoustic sensor based on a PP/PET diaphragm," *IEEE Sensors J.*, vol. 16, no. 9, pp. 3054–3058, May 2016.

[20] S. Dass and R. Jha, "Tapered fiber attached nitrile diaphragm-based acoustic sensor," *J. Lightw. Technol.*, vol. 35, no. 24, pp. 5411–5417, Dec. 15, 2017.

[21] M. Shimada, Y. Kinefuchi, and K. Takahashi, "Sleeve-type ultra miniature optical fiber pressure sensor fabricated by DRIE," *IEEE Sensors J.*, vol. 8, no. 7, pp. 1337–1341, Jul. 2008.

[22] Z. Gong, K. Chen, X. Zhou, Y. Yang, Z. Zhao, H. Zou, and Q. Yu, "High-sensitivity Fabry–Pérot interferometric acoustic sensor for low-frequency acoustic pressure detections," *J. Lightw. Technol.*, vol. 35, no. 24, pp. 5276–5279, Dec. 15, 2017.

[23] X. Fu, P. Lu, W. Ni, H. Liao, X. Jiang, D. Liu, and J. Zhang, "Phase interrogation of diaphragm-based optical fiber acoustic sensor assisted by wavelength-scanned spectral coding," *IEEE Photon. J.*, vol. 10, no. 3, pp. 1–11, Jun. 2018.

[24] W. Zhang, P. Lu, W. Ni, W. Xiong, D. Liu, and J. Zhang, "Gold-diaphragm based Fabry–Pérot ultrasonic sensor for partial discharge detection and localization," *IEEE Photon. J.*, vol. 12, no. 3, Jun. 2020, Art. no. 6801612.

[25] B. Liu, J. Lin, J. Wang, C. Ye, and P. Jin, "MEMS-based high-sensitivity Fabry–Pérot acoustic sensor with a 45° angled fiber," *IEEE Photon. Technol. Lett.*, vol. 28, no. 5, pp. 581–584, Mar. 1, 2016.

[26] E. Li, "Sensitivity-enhanced fiber-optic strain sensor based on interference of higher order modes in circular fibers," *IEEE Photon. Technol. Lett.*, vol. 19, no. 16, pp. 1266–1268, Aug. 15, 2007.

[27] T. B. Waluyo and D. Bayuwati, "An SMS (single mode–multi mode–single mode) fiber structure for vibration sensing," in *Proc. 2nd Int. Symp. Frontier Appl. Phys.*, Jakarta, Indonesia, 2016, pp. 1–6.

[28] Q. Wu, Y. Semenova, P. Wang, and G. Farrell, "The use of a bent singlemode-multimode-singlemode (SMS) fiber structure for vibration sensing," in *Proc. 21st Int. Conf. Opt. Fiber Sensors*, Ottawa, ON, Canada, May 2011, pp. 1–4.

[29] Y. Zhao, X.-G. Li, F.-C. Meng, and Z. Zhao, "A vibration-sensing system based on SMS fiber structure," *Sens. Actuators A, Phys.*, vol. 214, pp. 163–167, Aug. 2014.

[30] A. Sun, Y. Semenova, and G. Farrell, "A novel highly sensitive optical fiber microphone based on single mode-multimode-single mode structure," *Microw. Opt. Technol. Lett.*, vol. 53, no. 2, pp. 442–445, Feb. 2011.

[31] M. E. Efimov, M. Y. Plotnikov, A. V. Kulikov, M. V. Mekhrengin, and A. Y. Kireenkov, "Fiber-optic interferometric sensor based on the self-interference pulse interrogation approach for acoustic emission sensing in the graphite/epoxy composite," *IEEE Sensors J.*, vol. 19, no. 18, pp. 7861–7867, Sep. 2019.

[32] P. Wang, G. Brambilla, M. Ding, Y. Semenova, Q. Wu, and G. Farrell, "Investigation of single-mode-multimode-single-mode and single-mode-tapered-multimode-single-mode fiber structures and their application for refractive index sensing," *J. Opt. Soc. Amer. B, Opt. Phys.*, vol. 28, no. 5, pp. 1180–1186, May 2011.

[33] N. Lalam, W. P. Ng, Q. Wu, X. Dai, and Y. Q. Fu, "Perfluorinated polymer optical fiber for precision strain sensing based on novel SMS fiber structure," in *Proc. 10th Int. Symp. Commun. Syst., Netw. Digit. Signal Process. (CSNDSP)*, Prague, Czech Republic, Jul. 2016, pp. 8–10.

[34] X. Wang, K. Tian, L. Yuan, E. Lewis, G. Farrell, and P. Wang, "A high-temperature humidity sensor based on a singlemode-side polished multimode-singlemode fiber structure," *J. Lightw. Technol.*, vol. 36, no. 13, pp. 2730–2736, Jul. 1, 2018.

[35] C. B. Scruby, "An introduction to acoustic emission," *J. Phys. E, Sci. Instrum.*, vol. 20, no. 8, pp. 946–953, Aug. 1987.

[36] E. Howells and E. T. Norton, "Detection of partial discharges in transformers using acoustic emission techniques," *IEEE Trans. Power App. Syst.*, vol. PAS-97, no. 5, pp. 1538–1549, Sep. 1978.

[37] R. Harrold, "Ultrasonic spectrum signatures of under-oil corona sources," *IEEE Trans. Electr. Insul.*, vol. EI-10, no. 4, pp. 109–112, Dec. 1975.

[38] W. Sikorski, "Development of acoustic emission sensor optimized for partial discharge monitoring in power transformers," *Sensors*, vol. 19, no. 8, pp. 1–30, Apr. 2019.

[39] S. E. F. Masnan, A. Z. Zulkifli, N. M. Azmi, S. M. Akib, H. A. Razak, H. Arof, and S. W. Harun, "Steel beam compressive strain sensor using single-mode-multimode-single-mode fiber structure," *IEEE Photon. J.*, vol. 8, no. 1, pp. 1–6, Feb. 2016.

[40] B. Dong, M. Han, L. Sun, J. Wang, Y. Wang, and A. Wang, "Sulfur hexafluoride-filled extrinsic Fabry–Pérot interferometric fiber-optic sensors for partial discharge detection in transformers," *IEEE Photon. Technol. Lett.*, vol. 20, no. 18, pp. 1566–1568, Sep. 15, 2008.

[41] C. Gao, W. Wang, S. Song, S. Wang, L. Yu, and Y. Wang, "Localization of partial discharge in transformer oil using Fabry–Pérot optical fiber sensor array," *IEEE Trans. Dielectr. Electr. Insul.*, vol. 25, no. 6, pp. 2279–2286, Dec. 2018.

[42] C. Gao, L. Yu, Y. Xu, W. Wang, S. Wang, and P. Wang, "Partial discharge localization inside transformer windings via fiber-optic acoustic sensor array," *IEEE Trans. Power Del.*, vol. 34, no. 4, pp. 1251–1260, Aug. 2019.

[43] M. S. Naidu and V. Kamaraju, *High Voltage Engineering*. New Delhi, India: McGraw-Hill, 2013, pp. 1–467.

[44] M. F. Rahman, P. Nirgude, and N. R. Burjupati, "Effect of irregular-shaped Cu particles on transformer oil PD characteristics under varying electrode configurations," *IET Sci., Meas. Technol.*, vol. 13, no. 2, pp. 201–211, Mar. 2019.

[45] K. Firuzi, M. Vakilian, B. T. Phung, and T. Blackburn, "Transformer components impact on compatibility of measured PDs: Comparison of IEC60270 and RF methods," *High Voltage*, vol. 4, no. 1, pp. 33–40, Mar. 2019.

L. G. PAVAN KUMAR CHAGANTI received the B.Tech. degree in electrical and electronics engineering from Jawaharlal Nehru Technological University Kakinada (JNTUK), in 2013. He is currently pursuing the M.Phil. degree in electrical engineering with Universiti Teknologi Malaysia (UTM), Johor Bahru, Malaysia. From 2013 to 2017, he worked as a Project Associate and an Assistant Engineer with the High Voltage Laboratory, Indian Institute of Technology Madras. His research interests include cable insulation diagnostics, optical fiber sensors, and partial discharge measurements.

MOHD HAFIZI AHMAD (Member, IEEE) received the Ph.D. degree in high voltage engineering. His Ph.D. works are related to partial discharge measurement on insulation. He was formerly a Visiting Researcher with the University of Leicester, U.K. He is currently working as a Senior Lecturer and a Researcher with the Institute of High Voltage and High Current (IVAT), Universiti Teknologi Malaysia (UTM). In IVAT UTM, he also serves as a Testing and Calibration Manager and involved in many calibrations and testing jobs related to high voltage equipment. He is also a Senior Technical Advisor for Global Testing Services (M) Sdn Bhd. Moreover, he has conducted several trainings and talks on partial discharge fundamental and measurement on primary electrical equipment for industries and universities. In relation to partial discharge, he has conducted field and laboratory partial discharge measurement for transformer, switchgear, cable, and rotating machines using conventional and non-conventional methods. He is also a member of IET and CIGRE.

MOHAMED AFENDI MOHAMED PIAH received the B.Elect.Eng. degree from Universiti Teknologi Malaysia, in 1986, the M.Sc. degree in power system from the University of Strathclyde, U.K., in 1990, and the Ph.D. degree in high voltage engineering from Universiti Teknologi Malaysia, in 2004. He was appointed as an Assistant Director (Test and Calibration Division) of the Institute of High Voltage and High Current (IVAT) from 1996 to 2000, and the Deputy Director of IVAT from 2007 to 2009. He is currently an Associate Professor with the Faculty of Electrical Engineering, Universiti Teknologi Malaysia, and a Fellow Member of IVAT. He is also a Signatory of High Voltage Testing accreditation lab of ISO/IEC 17025. He is also the Head of the Department of Electrical Power, Faculty of Electrical Engineering. He has been involved in testing and calibration of high voltage equipments. His research interests include high voltage insulation diagnostic and co-ordination, electrical discharges, polymer nanocomposites insulating materials, and insulator condition monitoring.

MUHAMMAD YUSOF MOHD NOOR received the B.Eng. and M.Eng. degrees in electrical engineering from Universiti Teknologi Malaysia (UTM), Johor Bahru, in 2006 and 2008, respectively, and the Ph.D. degree from the University of New South Wales (UNSW), Sydney, in 2014. His Ph.D. work was related to the area of optical fiber sensor and application in biomedical engineering. He joined UTM in 2008, where he is currently a Senior Lecturer. His research interests include the development of fiber based sensing techniques and application of fiber sensing technology in engineering areas.

ASRUL IZAM AZMI received the B.Eng. and M.Eng. degrees in electrical engineering from Universiti Teknologi Malaysia (UTM), Johor Bahru, in 2001 and 2004, respectively, and the Ph.D. degree from the University of New South Wales (UNSW), Sydney, in 2012. His Ph.D. work was related to the area of optical fiber sensor and application in mechanical engineering. He joined UTM in 2002 as a Tutor, where he is currently a Senior Lecturer. He has been appointed as the Head for research group Lightwave Communication Research Group, UTM, since 2014. He then joined Jurutera Budiman (M&E) Sdn Bhd Consultant firm for industrial internship from September 2017 to November 2018. He went to Harbin Engineering University as a Visiting Researcher in March and July 2019. His research interests include optical sensor, including specialty fiber, fiber laser, fiber Brag grating, and spectroscopy based sensors.

● ● ●